electronics

MDPI

Article

Data-Driven Surrogate-Assisted Optimization of Metamaterial-Based Filtenna Using Deep Learning

Peyman Mahouti [1,*], Aysu Belen [2], Ozlem Tari [3], Mehmet Ali Belen [4], Serdal Karahan [5] and Slawomir Koziel [6,7]

[1] Department of Electronic and Communication Engineering, Yıldız Technical University, Istanbul 34220, Turkey
[2] Department of Hybrid and Electric Vehicles, Iskenderun Technical University, Hatay 31200, Turkey
[3] Department of Mathematics and Computer Science, İstanbul Arel University, Istanbul 34537, Turkey
[4] Department of Electric and Electronic Engineering, Iskenderun Technical University, Iskenderun 31200, Turkey
[5] Department of Automation, İstanbul University-Cerrahpaşa, Istanbul 34098, Turkey
[6] Department of Engineering, Reykjavik University, 102 Reykjavik, Iceland
[7] Faculty of Electronics, Telecommunications and Informatics, Gdansk University of Technology, 80-233 Gdansk, Poland
* Correspondence: pmahouti@yildiz.edu.tr

Abstract: In this work, a computationally efficient method based on data-driven surrogate models is proposed for the design optimization procedure of a Frequency Selective Surface (FSS)-based filtering antenna (Filtenna). A Filtenna acts as a module that simultaneously pre-filters unwanted signals, and enhances the desired signals at the operating frequency. However, due to a typically large number of design variables of FSS unit elements, and their complex interrelations affecting the scattering response, FSS optimization is a challenging task. Herein, a deep-learning-based algorithm, Modified-Multi-Layer-Perceptron (M2LP), is developed to render an accurate behavioral model of the unit cell. Subsequently, the M2LP model is applied to optimize FSS elements being parts of the Filtenna under design. The exemplary device operates at 5 GHz to 7 GHz band. The numerical results demonstrate that the presented approach allows for an almost 90% reduction of the computational cost of the optimization process as compared to direct EM-driven design. At the same time, physical measurements of the fabricated Filtenna prototype corroborate the relevance of the proposed methodology. One of the important advantages of our technique is that the unit cell model can be re-used to design FSS and Filtenna operating various operating bands without incurring any extra computational expenses.

Keywords: metamaterials; optimization; deep learning; frequency selective surfaces; filtering antenna

Citation: Mahouti, P.; Belen, A.; Tari, O.; Belen, M.A.; Karahan, S.; Koziel, S. Data-Driven Surrogate-Assisted Optimization of Metamaterial-Based Filtenna Using Deep Learning. *Electronics* **2023**, *12*, 1584. https://doi.org/10.3390/electronics12071584

Academic Editors: Xiongying Liu, Shaoqiu Xiao, Kai-Da Xu and Yi Fan

Received: 23 January 2023
Revised: 23 March 2023
Accepted: 26 March 2023
Published: 28 March 2023

1. Introduction

Metamaterials are materials that are artificially engineered by humans. The word itself is derived from the Greek 'meta' meaning 'beyond' and the Latin 'materia', which stands for 'material'. Metamaterials exhibit unusual properties that are generally different from their base materials occurring in nature [1]. In the realm of high-frequency electronics, they are often realized as a composition of materials such as metal and plastic to form elementary (or unit) cells. These are placed in a specific pattern, depending on the wavelength of the applications they are being devised for. The properties of metamaterials depend on the geometry/material parameters of the unit cells, their placement pattern, and orientation. Metamaterials possess remarkable properties that help manage electromagnetic waves by bending, absorbing, blocking, or increasing them and resulting in far better performance of the devices they are incorporated into as compared to those achievable with traditional materials [2,3].

With the phenomenal growth of mobile communication technology, there has been a similar increase in the electromagnetic interference of signals. For example, GSM signals create widespread interference in equipment used in locations such as hospitals, military workplaces, and railways [4–6]. This may lead to damage and operating issues for the affected equipment. Studies on the subject have shown that the most significant electromagnetic interference is due to GSM 900/1800 bands [7,8].

The upsurge in the usage of multifunctional modules has led to the development of filtering antennas (referred to as filtennas). These act as pre-filtering systems for multifunctional units. A communication system that includes a sensitive receiver has, at its front end, a band-pass RF filter. The filter separates the superfluous signals present out of the band from the signals needed for the system operation. When the antenna and the band-pass filter are combined into a single module enabling a pre-filtering process, filtering out of redundant signals becomes possible, even when these are stronger than the desired ones. The pre-filtered signal at the input stage will thus improve the signal-to-noise ratio in the receiver, enhancing the performance. At the same time, it will make the system more efficient and compact. Recent advancements in this field have examined the amalgamation of filter and antenna functions. One of the antennas with a built-in filter has been devised by using dual-post resonators [9]. Another study suggests a filtering antenna realized by a Substrate integrated waveguide structure [10]. Other studies investigated the employment of filters and microstrip patches in single-layer or multilayer substrates [11–13]. Frequency-selective surfaces (FSSs) constitute a class of meta-materials that may be one- or two-dimensional structures implemented on a dielectric substrate. They can be used in various applications such as the design of radomes, polarizers, beam splitters, and reflector antennas. They can also be used as radar absorbers. FSSs are especially useful for military purposes in aircraft, missiles, and ships where they can be used in antennas and for radar cross-section (RCS) reduction. The popularity of FSSs has increased tremendously with the burgeoning of communication systems. Strong electromagnetic interference (EMI) can seriously affect and damage electronic devices used for communication systems and necessitate the employment of anti-interference means. To achieve this, communication systems are amalgamated with FSSs. Despite their increasing popularity, there are surprisingly few studies conducted on the subject of the integration of antennas and FSSs. The very first mention of this technique can be found in [14]. However, therein it was used to boost the antenna radiation efficiency and was referred to as an artificial magnetic conductor for its use as a material with high impedance. Other studies have discussed multilayer FSS integration with open-end wave-guide radiator arrays but these specifically examine only the filtering ability of the integrated module [14–18].

Metamaterials have the disadvantage of possessing unwieldy configurations. Fabrication of these materials can also be a complicated process. However, researchers have found a way around this disadvantage by using metasurfaces to achieve the same manipulation of the front of an electromagnetic wave [19]. Metasurfaces are akin to metamaterials and feature a similar 2D design. They are made of unit cell elements laid out in a stipulated pattern that helps manipulate electromagnetic waves with innate properties such as negative refraction [20]. Another advantage of metasurfaces is that they are capable of prolonging the π phase span of an electric resonant plane, leading to a phase modulation of nearly 2π. As stipulated by the Huygens principle, this allows the wave-front to be deployed fully; both electric and magnetic surface currents are manipulated resulting in unidirectional scattering. Optimum efficiency is thus achieved in the transmission due to the manipulation ability of metasurfaces [21,22].

As mentioned earlier, FSSs have gradually become the structures of choice for communication systems in applications that require high-quality co-polarization with a low cross-polarization level over broad ranges of frequencies [23,24], especially for radars and antennas in military platforms such as aircraft, ships, and missiles, where it is imperative that they are not impacted by unnecessary external signals [25,26]. A powerful electromagnetic interference (EMI) can seriously affect electronic devices, even to the point

of destroying them. Therefore, an anti-interference element is crucial for the optimum operation of communication systems. This makes the integration of antenna and FSSs advantageous. Such a device can be designed as a single filtering antenna unit [27,28]. FSSs can also be printed on conductive materials or even the wall of the system itself by inserting another layer of printed or etched FSS pattern on the isolation material. A number of studies have examined various techniques of shielding GSM signals that are based on Double Square Loop (DSL) and double ring components [25,26]. There have been numerous other recommendations as well. One of these suggests the utilization of passive FSS designs within integrated modules whereby they can be used as a coating on the energy-saving glass. This approach may permit a selection of frequencies to be passed through while filtering out the unwelcome ones [29,30].

Designing a high-performance filtenna is a challenging undertaking. Filtennas need to exhibit high performance in various aspects such as appropriate allocation of the operating bands and their enhancement levels (regardless of whether they are single, dual, multiband, or ultra-wideband). In addition, filtenna development has to account for the structure size and to ensure low manufacturing costs. At the same time, the devices should be versatile to permit diverse applications [31]. A full-wave electromagnetic (EM) analysis is an indispensable design tool as it allows for precise characterization of the antenna structures. However, EM is computationally expensive, especially when combined with numerical procedures such as tolerance analysis or optimization. This aspect somewhat undermines the benefits of EM simulation as a reliable evaluation engine. A workaround for the high-cost issue is the incorporation of data-driven surrogate modeling methods. This approach has proven successful as a low-cost alternative for designing high-frequency systems in various contexts such as optimization of scattering parameters [32,33], reflection phase of reflectarray antennas [34], or design of microstrip filters [35]. The mentioned design procedure involves various Artificial Intelligence (AI) regression techniques, for instance, polynomial approximation, kriging, Support Vector Regression (SVR), Artificial Neural Networks (ANNs), and Deep Learning (DL) [36]. These methods are used to render an accurate mapping between the input space of the model and the targeted outputs.

This study employs data-driven surrogate modeling to enable low-cost design optimization of unit elements of FSS for the development of a filtenna. The objectives are to ensure a high radiation performance but also to maintain a small size, thereby fulfilling the space-related constraints of the target application. The training data samples for surrogate model construction are obtained from the 3D EM simulation model of a unit FSS element. The model input includes the operating frequency, geometrical design variables, and the radiation direction. The scattering parameters of the FSS unit cell are the model outputs. The hyper-parameters of the surrogate are identified using Bayesian Optimization (BO). Given the surrogate, the optimum design variables of the proposed filtenna are obtained using the Honey Bee Mating Optimization (HBMO) procedure directly optimizing the data-driven model. The goal is to develop an FSS unit element that can be positioned perpendicularly on the aperture of a horn antenna as a band-stop pre-filter for the 5-to-7 GHz frequency band. The numerical results demonstrate considerable (almost 90%) design speedup achieved with the proposed surrogate-assisted approach as compared to direct EM-driven design. Whereas, experimental validation of the filtenna corroborates the adequacy of the complete design procedure. One of the important advantages of the proposed technique is that the surrogate model rendered for optimization of the specific filtenna considered here may be re-used without incurring any extra computational to develop other designs, e.g., operating at different frequency bands.

2. Data-Driven Surrogate Model of Frequency Selective Surface Unit Element

Figure 1 shows a proposed 3D-printable unit element of the FFS. The material of choice is Polylactic acid (PLA) 1.75 mm 3D printing filament [37] featuring a dielectric constant of 2.4. Design variables of the cell and their ranges have been gathered in Table 1. A parametric analysis of the variables can be found in Figure 2. It can be noted that all

variables have significant effects on the resonant frequency of the element. To obtain the optimal design variables for a specified scattering parameter response, simultaneous optimization of the parameters is imperative, which has to be conducted in a global sense. However, direct EM-driven is extremely expensive in computational terms. In this work, to reduce CPU costs, Artificial Intelligence (AI)-based regression models are employed. The prerequisite for maintaining low costs is that both the training and test (holdout) data sets must be reasonably small. Here, the model is constructed using 500 Latin-Hypercube Sampling (LHS)-generated training samples and 100 hold-out samples. Each of the samples is a vector of scattering parameters evaluation within the frequency range from 2 to 10 GHz with the step of 0.1 GHz. To reduce the total number of design variables/dimensions of the problem, some of the design variables are taken as constant or are functions of other variables as follows: $L = W$, $L_1 = 0.9L$, $W_1 = 0.9W - 2L_2$.

For comparison, a number of state-of-the-art modeling methods are used: (i) Multi-Layer Perceptron, (ii) Support Vector Regression Machine, (iii) Gradient Boosted Tree; (iv) Keras Deep Residual Neural Network (NN) Regressor, (v) Gaussian Process Regression(vi) Modified Multi-Layer Perceptron (M2LP) [38]. All these methods are used to construct behavioral models of the FSS unit cell scattering parameters with respect to the design variables defined in Table 1. The predictive power of the model is measured using the Relative Mean Error (RME)

$$RME = \frac{1}{N}\sum_{i=1}^{N}\frac{|T_i - P_i|}{|T_i|} \tag{1}$$

where T_i and P_i stand for the target and model-predicted value of ith sample, whereas N is the total number of samples.

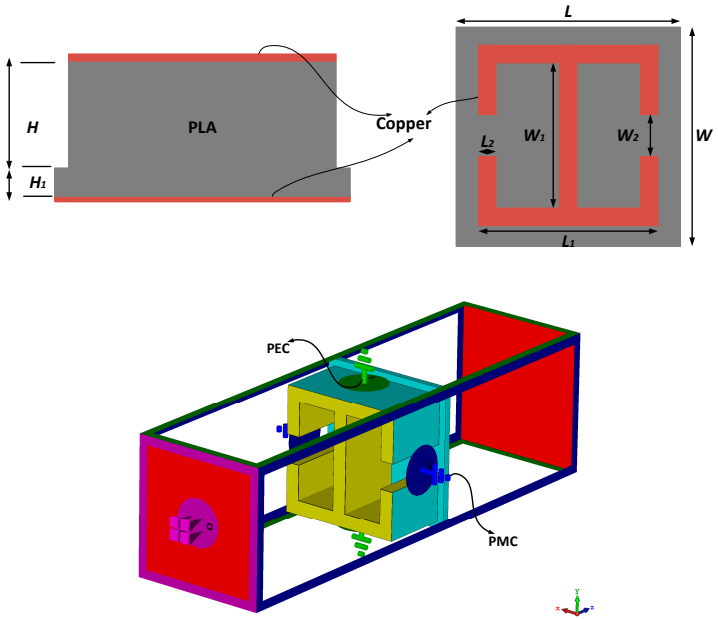

Figure 1. Schematic views of the proposed 3D FSS unit element.

Table 1. Design variables of the FSS unit element and their lower and upper bounds in [mm].

Parameter	Lower Boundary	Upper Boundary
H	1	20
H_1	0.5	3
L_2	0.5	5
W_2	1	10

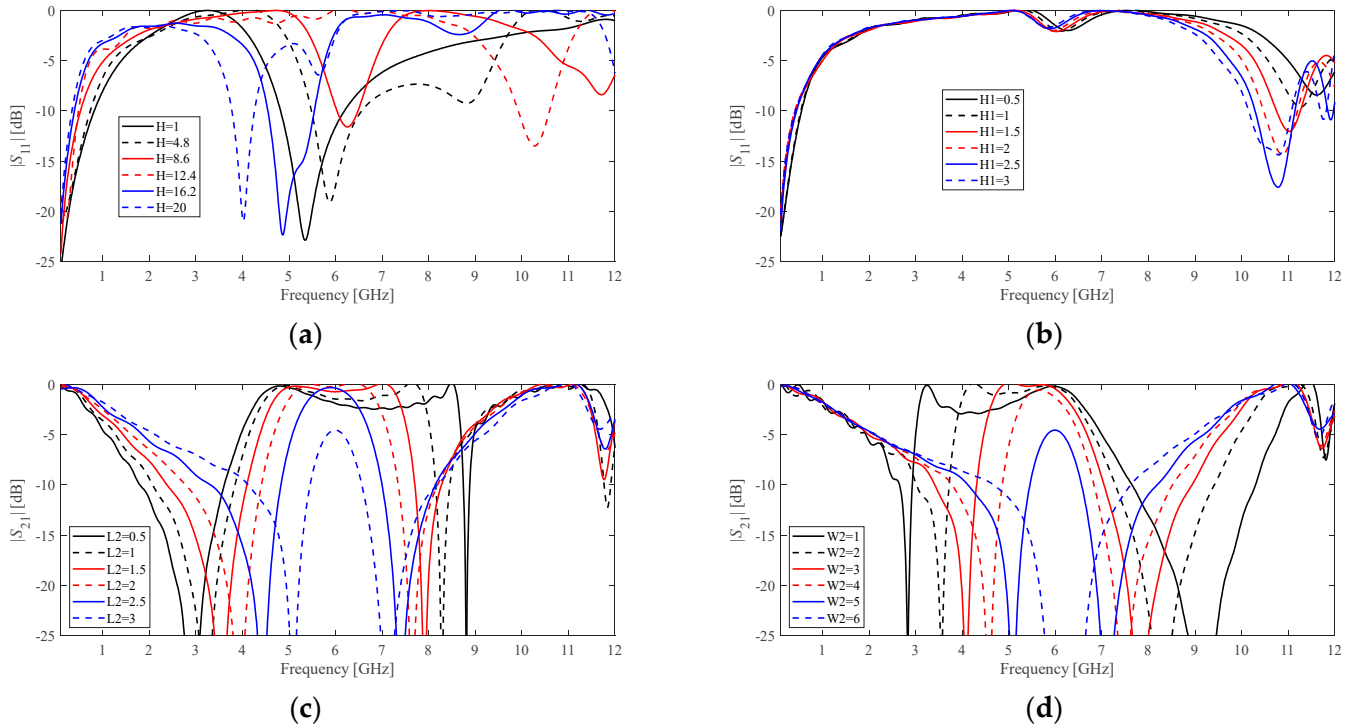

Figure 2. Parametric analysis of the FSS unit element for: (**a**) $|S_{11}|$ (as a function of H); (**b**) $|S_{11}|$ (as a function of H_1); (**c**) $|S_{21}|$ (as a function of L_2); (**d**) $|S_{21}|$ (as a function of W_2). All the variables are taken as constant values while the selected one is swept, H = 10.5, H_1 = 2, L_2 = 2, and W_2 = 4, all variables are in [mm].

The results shown in Table 2 are based on K-fold cross-validation (K = 5). While the K-fold is used to identify the best model based on the training process, the holdout data set is used to estimate the over-fitting performance of the surrogates. The hyper-parameters of the models are determined using Bayesian Optimization with maximum objective evaluations epoch set to 30. Based on data in Table 2, although the best performance is achieved by the FCRM surrogate model (4.1% hold-out error), the required training time for the model and its optimization is more than twice the time for the M2LP surrogate model, which achieves a hold-out error of 4.7%. Both models exhibit a similar error rate of less than 5%, both according to cross-validation and the hold-out test, which suggest that they are not only well-trained but also not over-fit. Thus, in overall performance comparison, the M2LP model is evaluated as a better solution from the perspective of overall computational efficiency. Here, it is worth mentioning that there are other types of approaches for modeling FSS unit elements such as the usage of equivalent circuit models [39] or physics-based models [40]. However, these methods have major limitations. They are computationally intensive, which prevents their direct use for circuit design. In most cases, it is inevitable to introduce simplifying assumptions in order to make the model computationally tractable [39]. Consequently, in this work, to ensure computational efficiency, a Deep-Learning-based surrogate modeling approach is taken into consideration, which exhibits excellent generalization capability even when working with small amounts of data. Consequently, the M2LP model will be employed for filtenna design as elaborated on in Section 3.

Table 2. Performance comparison of data-driven surrogate models.

Model	Hyper-Parameters	K-Fold/Holdout	Total Training Time [Minutes]
MLP	Hidden Layer size-2; Hidden Layer Neurons sizes 15–20; Activation function sigmoid	6.0%/7.5%	~17.5
SVRM	Kernel-function: Radial, Type: Epsilon, Epsilon: 0.1.	6.4%/8.1%	~14.0
Gradient Boosted Tree	Learning-rate = 0.045; Depth: 5; N. estimators: 4800	7.6%/8.4%	~8.5
Keras Deep Residual NN Regressor	N. Layers:2; N. Neurons: 512–512	4.6%/5.4%	~27.0
Gaussian Process Regression	Kernel-function: ard-matern3/2; Prediction-method: Block-coordinate-descent; block-size: 750	5.4%/6.2%	~27.0
M2LP	Depth: 3, initial Neuron N.: 64	3.9%/4.7%	~21.0
Convolutional Neural Networks	N. Layers:3; N. Neurons: 64–128-256	4.3%/5.2%	~29.0
FCRM [36]	Block size = 3; Sublock = Fully Connect + Leak ReLU Sublock neurons Number = {256, 1024, 1024})	3.2%/4.1%	~42.5

3. Surrogate-Assisted Design Optimization of Filtenna

In this section, the M2LP surrogate model is used for the design optimization of the filtenna. The search engine is the Honey Bee Mating Optimization [41] (HBMO), a meta-heuristic algorithm based on the mating strategy of Honey Bees. HBMO is a population-based procedure capitalizing on the evolutionary algorithm principles. In this particular routine, the fittest individual (candidate solution) becomes the Queen Bee. The quality of design corresponding to a particular individual (parameter vector) determine the fertility rate of the Queen Bee or queen candidates. At each generation, the quality of the newly created individuals is compared to that of the Queen. The superior individual becomes the new Queen itself, affecting the creation of new individuals for the subsequent iteration. This outline corresponds to the global part of the optimization process. The operating details of the algorithm can be found in the literature [41]. Another parameter that significantly affects the fitness of Queen Bees is "Royal Jelly". This nutrition can extend the life of a common bee from thirty days to two years which is the key to a bee becoming a Queen. This phenomenon also is being used in the HBMO protocol to foster local optimization. Thus, HBMO is a hybrid search protocol that combines both global and local searches for finding the optimal solution to the problem.

It should be mentioned that although a selection of the optimization protocol is generally important, in our particular case, it is of secondary relevance. Having a fast surrogate model, any global search procedure can be used and set up with an essentially unlimited computational budget. With a model evaluation time of about 1 ms, even hundreds of thousands of objective function evaluations would not entail meaningful costs as compared to even a single EM analysis of the FSS unit cell. On the other hand, direct EM-driven optimization is normally prohibitive. The EM simulation time of the unit cell in our case is around 1 min. With a computational budget of, say 5000 objective function evaluations (still rather conservative), the CPU time of the search process reaches 80 h.

The objective function utilized to optimize the FSS is defined as follows:

$$x^* = \underset{x}{\operatorname{argmin}}[w_1 C_1(x) + w_2 C_2(x) + w_3 C_3(x)] \quad (2)$$

where

$$C_1(x) = \min\{ f \in [f_{c2}, f_{c3}] : |S_{11}(x, f)| \} \quad (3)$$

$$C_2(x) = \min\{ f \in [f_{c1}, f_{c2}] : |S_{21}(x, f)| \} \quad (4)$$

$$C_2(x) = \min\{ f \in [f_{c3}, f_{c4}] : |S_{21}(x, f)| \} \quad (5)$$

Here, x is the vector of design variables of $\boldsymbol{x}$= $[W_1\ L_1\ S_1\ H_2]^T$. $[f_{c2}, f_{c3}]$ is the target operating band, whereas $[f_{c1}, f_{c2}]$ and $[f_{c3}, f_{c4}]$ are the rejection bands, where the transmission coefficient is to be minimized. $[w_1, w_2, w_3]$ are weighing coefficients to adjust the importance of the terms C_j, j = 1, 2, 3. Here, we put equal weights, i.e., w_j = 1, j = 1, 2, 3. The C_1 and C_3 determine the worst-case transmission for the frequency ranges $[f_{c1}, f_{c2}]$ and $[f_{c3}, f_{c4}]$. The term C_2 is the maximum in-band reflection within the target band $[f_{c2}, f_{c3}]$. Here, we set f_{c1} = 3 GHz, f_{c2} = 5 GHz, f_{c3} = 7 GHz, f_{c4} = 9 GHz. The optimal parameters of the FSS unit element for the operating band of 5–7 GHz are H = 10, H_1 = 1, L_1 = 18, L_2 = 2, W_1 = 14, W_2 = 4, and W = L = 20 [mm]. The control parameters of the HBMO algorithm were taken as follows: the maximum number of iterations 15; the number of drone bees 20, the Royal Jelly step size ±0.1 [41]. Figure 3 shows a comparison of the M2LP-model-predicted and EM-simulated FSS responses at the optimum design found by HBMO. The agreement between the two sets of data is excellent. In the next section, for finalizing the filtenna design, the obtained unit element will be used to form an array to be placed in the aperture of a horn antenna.

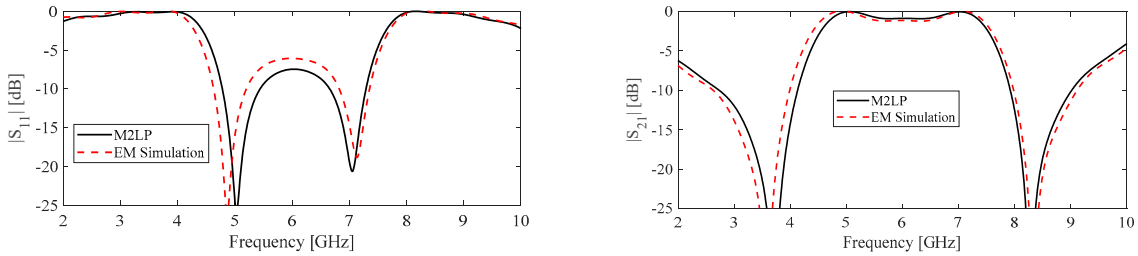

Figure 3. EM-simulated and M2LP-predicted responses: (**a**) $|S_{11}|$, (**b**) $|S_{21}|$, responses of optimally selected FSS element. H = 10, H_1 = 1, L_1 = 18, L_2 = 2, W_1 = 14, W_2 = 4, and W = L = 20 all in [mm].

4. Experimental Results

The optimally designed FSS unit element has been manufactured using 3D printing technology. A 3-by-3 array has been assembled as shown in Figure 4. Although it is possible to extend the performance of the design with a larger size of the FSS array (Figure 5a,b), for the selected horn antenna design [42], an FSS array design with a 3-by-3 element is selected to have a smaller module volume size. The top layer of the 3D-printed FSS array is metal-coated using copper tape and placed into the aperture of a ready-to-use horn antenna. Figure 5a,b show the scattering response of the unit element and the FSS array. It can be observed that the unit element response is preserved by the array configuration. The measured reflection and maximum gain radiation of the filtenna and horn antenna without an FSS array have been shown in Figure 5c,d. As for further analyses of the performance of the FSS design, the effect of oblique incident angles are also studied in Figure 5e,f. As can be seen from the measurement results, the filtenna enhances the radiation characteristic of the horn antenna within the target operating band of 5-to-7 GHz, while the outer bands of the antenna are reduced by almost 7 dBi (Table 3). The 3D printed filtenna then is metalized using copper tapes. It is worth mentioning that surface roughness is a parameter that might deteriorate the overall performance of a design [43–45]. However, as can be seen from the simulated results and measurements, the surface roughness on the prototype FSS can be neglected. Consequently, the radiation characteristic of the antenna is enhanced by almost 2 dBi at the desired operating range but also a pre-filtering characteristic is obtained for the unwanted frequencies (Figure 6). Thus, with the proposed approach, the

major obstacle of geometry parameter adjustment of the FSS unit cell to ensure proper electrical performance and to maintain the required size, has been achieved through a computationally-efficient design optimization procedure. It should be emphasized that accurate evaluation of the cell requires EM analysis, which is computationally heavy. In particular, direct EM-based optimization is usually impractical. With the typical simulation time of around 1 min and global optimization of the FSS cell requiring at least 5000 analyzes, the overall design time exceeds 80 CPU hours. The approach adopted here employs a deep-learning-based model M2LP to create a fast surrogate. M2LP has been found superior to commonly used state-of-the-art techniques such as MLP, SVRM, Boosted Trees, Depp NN, and Gaussian Process regression, in terms of predictive power. Here, it is worth mentioning that, there other data-driven surrogate approaches such as inverse modeling [46] can be used to yield high-performance designs. However, these methods also exhibit drawbacks, such as limited Design of Freedom (DOF) for variables of the problem, where the same targeted performance might have more than one (or even dozens of) possible solutions, effectively leading to non-uniqueness issues. In particular, the model may fail to render a unique response due to the failure in adjusting the model weighting coefficients for the same input and different outputs. Consequently, the designer has to cancel out or take constant values of some of the design variables that would reduce the DOF and performance of the obtainable optimal FSS design. The direct (or forward) modeling approach is not affected by the aforementioned uniqueness issues. On the other hand, the disadvantage of forward-modeling-based methods is the necessity of often time-consuming model optimization to determine the optimal solution for the target performance response. Yet, if the forward model is computationally cheap, as is the case in this work, the said drawback has been effectively eliminated: the unit cell optimization cost becomes negligible. As each (model-predicted) function evaluation takes less than one millisecond, even an optimization process involving 10,000 objective function calls would be shorter than one minute, the time corresponding to a single EM analysis of the unit cell. The obtained numerical and experimental data indicate that the proposed design approach is highly reliable and computationally efficient. The estimated speedup with respect to direct EM-driven optimization using population-based methods is almost 90%. Additionally in Table 4, the performance of the optimal design Filtenna is compared with state-of-the-art designs reported in the literature.

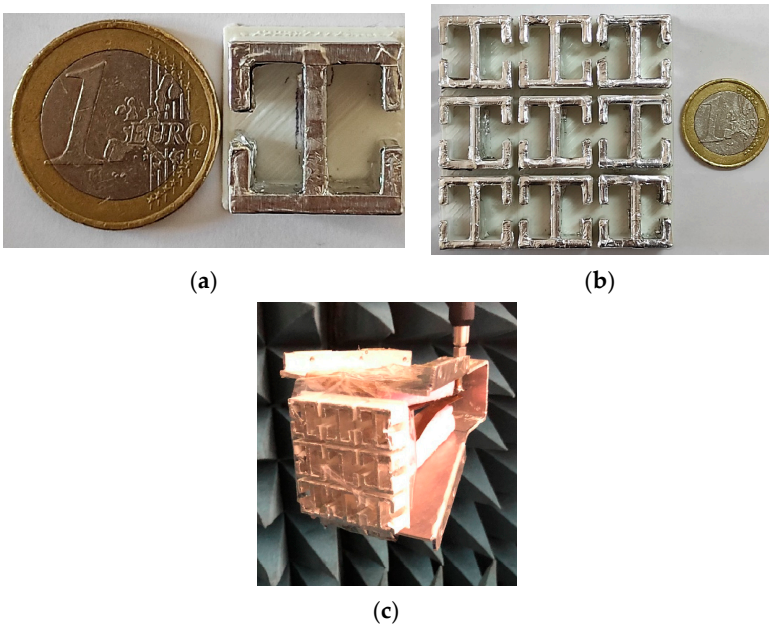

(**a**) (**b**)

(**c**)

Figure 4. Photograph of the prototyped filtennas: (**a**) FSS unit cell, (**b**) FSS array design, and (**c**) filtenna structure.

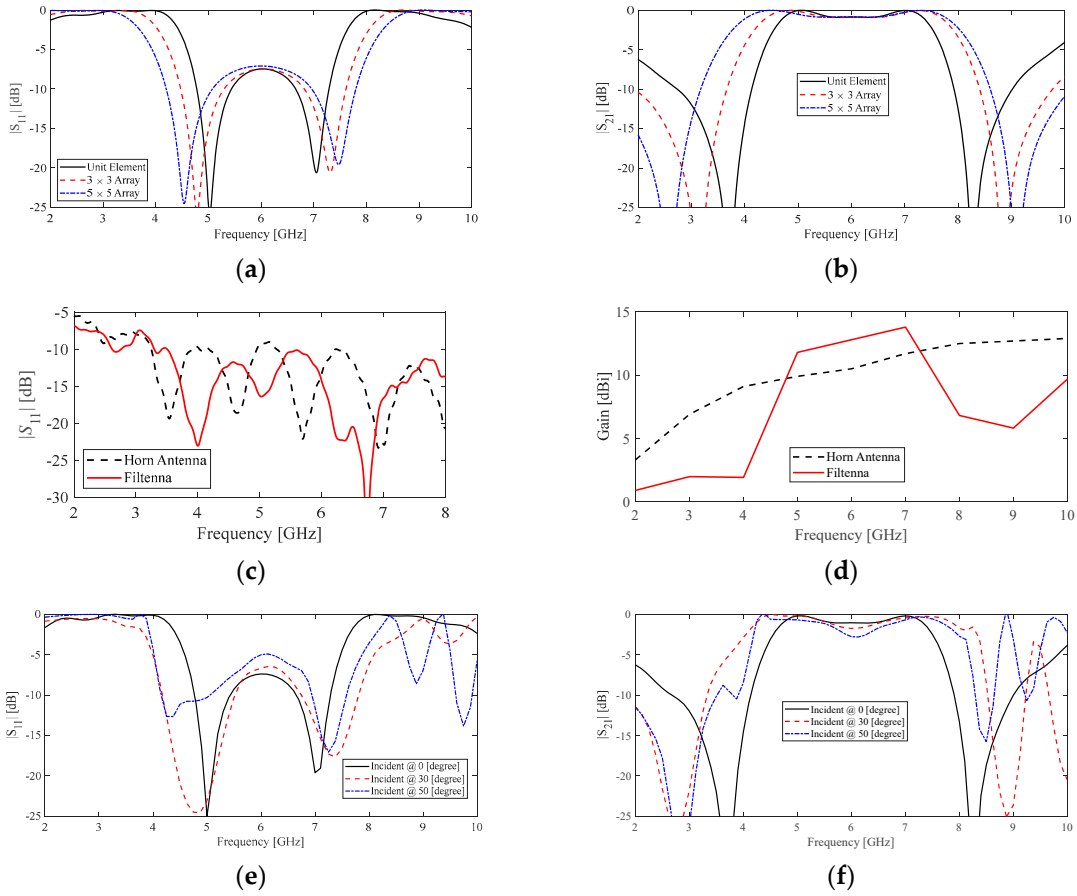

Figure 5. Scattering parameters responses of the 3D unit element and proposed filtenna: (**a**) simulated $|S_{11}|$, (**b**) simulated $|S_{21}|$, (**c**) measured $|S_{11}|$, (**d**) gain, simulated (**e**) $|S_{11}|$, and (**f**) $|S_{21}|$ for different oblique incidences.

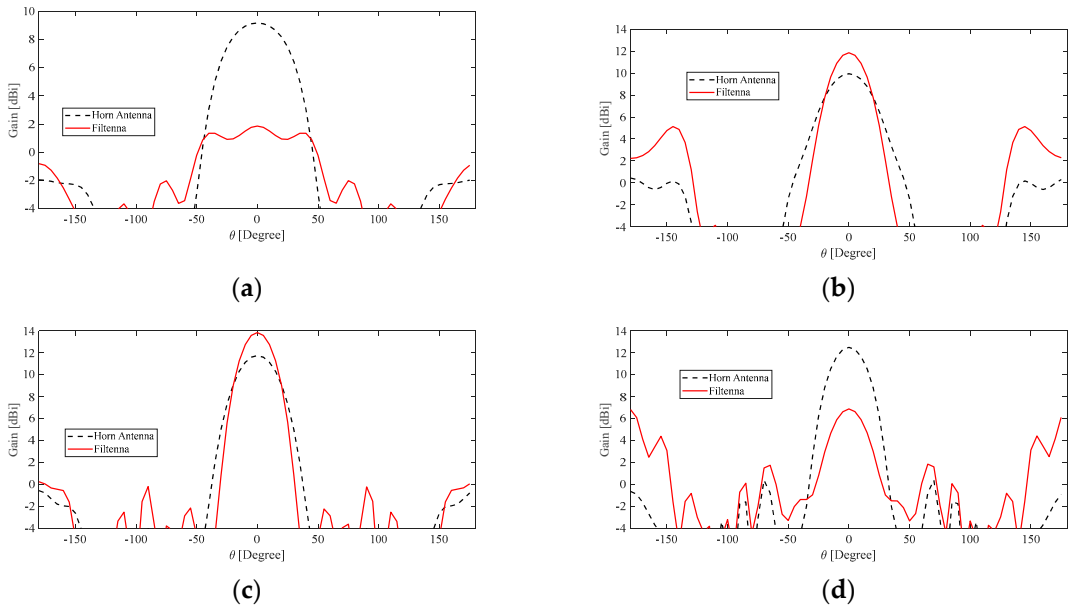

Figure 6. Measured radiation pattern (@ $\phi = 90°$) of the horn and filtenna designs at (**a**) 4 GHz, (**b**) 5 GHz, (**c**) 7 GHz, and (**d**) 8 GHz.

Table 3. Measured maximum gain [dBi].

Frequency [GHz]	TEM	FILTENNA
4	9.1	1.9
5	9.9	11.8
6	10.5	12.8
7	11.7	13.8
8	12.5	6.8

Table 4. Comparison of gain enhancement of state-of-the-art filtennas operating in similar frequency bands.

Work	Operating Band [GHz]	Design Size [mm]	Gain Alteration [dBi]/[GHz]				
			4	**5**	**6**	**7**	**8**
This work	4–8	60 × 60	–7.2	1.9	2.3	2.1	–5.7
[47]	5–15	16 × 16	0	1	0.5	0	0.5
[48]	1–15	60 × 100	2	2.5	3	3	4
[49]	2–13	25 × 73.5	1	1.5	2	2.5	2.7
[50]	2–13	100 × 100	0	5	4.5	5	2
[51]	3–12	80 × 800	2	1	3	2	3
[52]	6–18	90 × 90	—	—	4	5	5.5
[53]	8–12	114 × 114	—	—	—	—	1.5
[54]	8–18	106 × 16	—	—	—	—	2
[55]	6–12	22 × 20	—	—	1	0	1.5

5. Conclusions

Herein, computationally-efficient design optimization of an FSS-based filtering antenna using data-driven surrogate models has been proposed. Our methodology employs a deep-learning-based model M2LP to create a fast surrogate, which is also found to be superior to benchmark models reported in the literature in terms of predictive power. In our case, the FSS has been optimized using the HBMO algorithm. The HBMO routine has been deployed to carry out design optimization of geometry parameters of printable FSS for a filtenna operating in the 5-to-7 GHz range. Experimental validation of the filtenna has been carried out by fabricating the FSS array in the 3D printing process and placing it on the aperture of the horn antenna. The filtenna achieves a pre-filtering performance of up to 7 dBi in the rejecting band. Further, it enhances the gain characteristic in the pass band (5–7 GHz) by up to 2 dBi. The obtained numerical and experimental data indicate that the proposed design approach is highly reliable and computationally efficient where the total computational cost of the optimization procedure is reduced by almost 90%. Another advantage of the presented method is the possible re-usability of the surrogate model, which represents the FSS unit cell over broad ranges of geometry parameters and frequencies. Consequently, it can be reused to design filtennas under a variety of scenarios involving different geometric constraints and target operating bands without any extra computational investments. The future work will be focused on extending the applicability range of the discussed methodology to multi-layer FSSs intended for the development of higher performance filtennas.

Author Contributions: Conceptualization, P.M., M.A.B. and S.K. (Slawomir Koziel); methodology, P.M. and O.T.; data generation, M.A.B. and A.B.; investigation, S.K. (Serdal Karahan), O.T. and P.M.; benchmarking models, A.B. and S.K. (Serdal Karahan); writing—original draft preparation, S.K.

(Slawomir Koziel), O.T. and P.M.; writing—review and editing, S.K. (Slawomir Koziel) and P.M.; visualization, M.A.B. and A.B.; supervision, O.T., M.A.B. and P.M.; project administration, M.A.B. and P.M. All authors have read and agreed to the published version of the manuscript.

Funding: This work had been supported by the Norway Grants 2014–2021 via the National Centre for Research and Development, grant NOR/POLNOR/HAPADS/0049/2019-00. and also had been supported in part by the Icelandic Centre for Research (RANNIS) Grant 217771.

Data Availability Statement: The datasets generated during and/or analysed during the current study are available from the corresponding author on reasonable request.

Acknowledgments: The authors would like to thank Aktif Neser, for making CST Microwave Studio available. The research leading to these results has received funding from the Norway Grants 2014–2021 via the National Centre for Research and Development, grant NOR/POLNOR/HAPADS/0049/2019-00. This work was also supported in part by the Icelandic Centre for Research (RANNIS) Grant 217771.

Conflicts of Interest: The authors declare no conflict of interest.

References

1. Engheta, N.; Ziolkowski, R.W. *Metamaterials: Physics and Engineering Explorations*; John and Wiley and Sons: Hoboken, NJ, USA, 2006.
2. Sichao, Q.; Sheng, P. Microwave and acoustic absorption metamaterials. *Phys. Rev. Appl.* **2022**, *17*, 047001.
3. Hussain, M.; Awan, W.A.; Alzaidi, M.S.; Hussain, N.; Ali, E.M.; Falcone, F. Metamaterials and Their Application in the Performance Enhancement of Reconfigurable Antennas: A Review. *Micromachines* **2023**, *14*, 349. [CrossRef] [PubMed]
4. Lawrentschuk, N.; Bolton, D.M. Mobile Phone Interference with Medical Equipment and its Clinical Relevance: A Systematic Review. *Med. J. Aus.* **2004**, *181*, 145–149. [CrossRef] [PubMed]
5. Rouco, A.; Cota, N.; Beire, A.R.; Serrador, A. Public Mobile Wideband Networks Interference Impact Assessment on Railways GSM-R Network. In Proceedings of the 2022 International Conference on Electrical, Computer and Energy Technologies (ICECET), Prague, Czech Republic, 20–22 July 2022; pp. 1–6.
6. Wiklundh, K. Interference challenges for industry communication. In *PDF Presentation Slides from Keynote at WFCS*; IEEE: Sundsvall, Sweden, 2019.
7. Iskra, S.; Thomas, B.W.; McKenzie, R.; Rowley, J. Potential GPRS 900/1800 MHz and WCDMA 1900 MHz interference to medical devices. *IEEE Trans. Biomed. Eng.* **2007**, *54*, 1858–1866. [CrossRef]
8. Genç, O.; Bayrak, M.; Yald, E. Analysis of the effects of GSM band-stop the electromagnetic pollution in the RF spectrum. *Prog. Electromagn. Res.* **2010**, *101*, 17–32. [CrossRef]
9. Alves, A.A.C.; da Silva, L.G.; Vilas Boas, E.C.; Spadoti, D.H.; Cerqueira, S.A. Continuously frequency-tunable horn filtennas based on dual-post resonators. *Int. J. Anten. Prop.* **2019**, *2019*, 6529343. [CrossRef]
10. Kumar, A.; Althuwayb, A.A. SIW Resonator-Based Duplex Filtenna. *IEEE Ant. Wire. Prop. Let.* **2021**, *20*, 2544–2548. [CrossRef]
11. Wang, W.; Jin, H.; Yu, W.; Zhang, X.H.; Wu, F.; Chin, K.-S.; Luo, G.Q. A Single-Layer Dual-Circularly Polarized SIW-Cavity-Backed Patch Filtenna With Wide Axial-Ratio Bandwidth. *IEEE Ant. Wire. Prop. Let.* **2021**, *20*, 908–912. [CrossRef]
12. Xiao, J.K.; Liu, X.-Q.; Li, X.-F. Four-port MIMO Filtenna Based on Multi-layer Suspended Coplanar Waveguide. In Proceedings of the 2021 IEEE International Workshop on Electromagnetics: Applications and Student Innovation Competition (iWEM), Guangzhou, China, 7–9 November 2021; pp. 1–3.
13. Tang, M.-C.; Li, D.; Chen, X.; Wang, Y.; Hu, K.; Ziolkowski, R.W. Compact, Wideband, Planar Filtenna with Reconfigurable Tri-Polarization Diversity. *IEEE Trans. Ant. Prop.* **2019**, *67*, 5689–5694. [CrossRef]
14. Erdemli, Y.E.; Sertel, K.; Gilbert, R.A.; Wright, D.E.; Volakis, J.L. Frequency selective surfaces to enhance performance of broad band reconfigurable arrays. *IEEE Trans. Antennas Propag.* **2002**, *50*, 1716–1724. [CrossRef]
15. Chou, H.-H.; Ke, G.-J. Narrow Bandpass Frequency Selective Surface With High Level of Angular Stability at Ka-Band. *IEEE Microw. Wire. Comp. Lett.* **2021**, *31*, 361–364. [CrossRef]
16. Guo, Q.; Li, Z.; Su, J.; Song, J.; Yang, l.Y. Active Frequency Selective Surface With Wide Reconfigurable Passband. *IEEE Access* **2019**, *7*, 38348–38355. [CrossRef]
17. Lalbakhsh, A.; Afzal, m.U.; Esselle, K.P.; Smith, S.L. All-Metal Wideband Frequency-Selective Surface Bandpass Filter for TE and TM Polarizations. *IEEE Trans. Ant. Prop.* **2022**, *70*, 2790–2800. [CrossRef]
18. De Sabata, A.; Matekovits, L.; Buta, A.; Dassano, G.; Silaghi, A. Frequency Selective Surface for Ultra-Wide Band Filtering and Shielding. *Sensors* **2022**, *22*, 1896. [CrossRef] [PubMed]
19. Yu, N.; Genevet, P.; Kats, M.A.; Aieta, F.; Tetienne, J.P.; Capasso, F.; Gaburro, Z. Light propagation with phase discontinuities: Generalized laws of reflection and refraction. *Science* **2011**, *334*, 333–337. [CrossRef]
20. Shelby, R.A.; Smith, D.R.; Schultz, S. Experimental verification of a negative index of refraction. *Science* **2001**, *292*, 77–79. [CrossRef]
21. Pfeiffer, C.; Grbic, A.A. Metamaterial huygens' surfaces: Tailoring wave fronts with reflectionless sheets. *Phys. Rev. Lett.* **2013**, *110*, 197401. [CrossRef]

22. Tsilipakos, O.; Koschny, T.; Soukoulis, C.M. Antimatched electromagnetic metasurfaces for broadband arbitrary phase manipulation in reflection. *ACS Photonics* **2018**, *5*, 1101–1107. [CrossRef]
23. Farooq, U.; Shafique, M.F.; Iftikhar, A.; Mughal, M.J. Polarization Insensitive Tri-Band FSS for RF Shielding at Normal and Higher Temperatures by Retrofitting on Ordinary Glass Windows. *IEEE Trans. Ant. Prop.* **2023**, 1. [CrossRef]
24. Dai, X.W.; Zhang, Y.H.; Yu, W.; Liu, L.; Luo, G.Q. A Broadband Low-Profile Dual-Circularly Polarized Reflect-Array Based on a Single-Layer Microstrip Patch for Ka-Band Application. *IEEE Trans. Ant. Prop.* **2023**, 1. [CrossRef]
25. Liu, X.; Chen, Z.; Feng, G.; Song, J.; Liu, Y.; Tian, D.; Sun, F.; Liu, Y.; Fei, H.; Yang, Y. Ultra-Wideband Terahertz Absorber Based on Metal–Graphene Hybrid Structure. *Mater. Today Commun.* **2023**, *34*, 105185. [CrossRef]
26. Li, J.; Shi, L.; Chen, H.; Qu, L.; Yi, Y.; Zhang, Q.; Fu, S.; Ma, Y.; Wang, J. High Angular Stability and Polarization Insensitive Optically Transparent Bandpass Frequency Selective Surface Based on Micro Copper Mesh. *Optics Comm.* **2023**, *536*, 129365. [CrossRef]
27. Luo, G.Q.; Hong, W.; Chen, H.; Tang, H.J.; Xin, J.; Yin, X.; Kuai, Z.Q.; Wu, K. Filtenna consisting of horn antenna and substrate integrated waveguide cavity FSS. *IEEE Trans. Antennas Propag.* **2007**, *55*, 92–98. [CrossRef]
28. Mahouti, P.; Güneş, F.; Belen, M.A.; Çalışkan, A.; Demirel, S.; Sharipov, Z. Horn antennas with enhanced functionalities through the use of frequency selective surfaces. *Int. J. RF Microw. Comp. Aided Eng.* **2016**, *26*, 287–293. [CrossRef]
29. Kiani, G.; Olsson, L.; Karlsson, A.; Esselle, K.; Nilsson, M. Cross-dipole band-pass frequency selective surface for energy-saving glass used in buildings. *IEEE Trans. Antennas Propag.* **2011**, *59*, 520–525. [CrossRef]
30. Seager, R.D.; Chauraya, A.; Bowman, J.; Broughton, M.; Philpott, R.; Nimkulrat, N. Fabric based frequency selective surfaces using weaving and screen printing. *Electron. Lett.* **2013**, *49*, 1507–1509. [CrossRef]
31. Imbriale, W.A.; Boccia, L. *Space Antenna Handbook*; John and Wiley and Sons: Hoboken, NJ, USA, 2012.
32. Pietrenko-Dabrowska, A.; Koziel, S. Fast EM-driven parameter tuning of microwave circuits with sparse sensitivity updates via principal directions. *Knowl. Based Syst.* **2022**, *252*, 109388. [CrossRef]
33. Koziel, S.; Pietrenko-Dabrowska, A.; Ullah, U. Tolerance-Aware Optimization of Microwave Circuits by Means of Principal Directions and Domain-Restricted Metamodels. *IEEE Trans. Microw. Theory Tech.* **2022**, *70*, 4085–4093. [CrossRef]
34. Çalışkan, A.; Güneş, F. 3D EM Data-driven Artificial Network-based Design Optimization of Circular Reflectarray Antenna with Semi-elliptic Rings for X-band Applications. *Microw. Opt. Techn. Lett.* **2021**, *64*, 537–543. [CrossRef]
35. Uluslu, A. Design of Microstrip Filter by Modeling with Reduced Data. *App. Comput. Electrom. Soc. J.* **2021**, *36*, 1453–1459. [CrossRef]
36. Koziel, S.; Mahouti, P.; Calik, N.; Belen, M.A.; Szczepanski, S. Improved modeling of microwave structures using performance-driven fully-connected regression surrogate. *IEEE Access* **2021**, *9*, 71470–71481. [CrossRef]
37. PLA 1.75 mm 3D Printing Filament. Available online: https://cel-uk.com/shop/pla/ (accessed on 24 November 2022).
38. Calik, N.; Belen, M.A.; Mahouti, P. Deep learning base modified MLP model for precise scattering parameter prediction of capacitive feed antenna. *Int. J. Numer. Model.* **2020**, *33*, e2682. [CrossRef]
39. Simruni, M.; Jam, S. Design of High Gain, Wideband Microstrip Resonant Cavity Antenna Using FSS Superstrate with Equivalent Circuit Model. *AEU Int. J. Electr. Comm.* **2019**, *112*, 152935. [CrossRef]
40. El-Ghazaly, S.M. Heterojunction Field Effect Transistors. In *Encyclopedia of Materials: Science and Technology*; Elsevier: Amsterdam, The Netherlands, 2001; pp. 3760–3767, ISBN 9780080431529.
41. Güneş, F.; Demirel, S.; Mahouti, P. Design of a front–end amplifier for the maximum power delivery and required noise by HBMO with support vector microstrip model. *Radioengineering* **2014**, *23*, 134–143.
42. Keskin, A.K.; Senturk, M.D.; Çalişkan, A.; Türk, A.S. UWB Compact TEM Ridged Horn Antenna. In Proceedings of the Annual Review of Progress in Applied Computational Electromagnetics, Jacksonville, FL, USA, 23–27 March 2014; pp. 114–118.
43. Genc, A.; Basyigit, I.B.; Colak, B.; Helhel, S. Investigation of the Characteristics of Low-Cost and Lightweight Horn Array Antennas with Novel Monolithic Waveguide Feeding Networks. *AEU Int. J. Electr. Comm.* **2018**, *89*, 15–23. [CrossRef]
44. Decrossas, E.; Reck, T.; Lee, C.; Jung-Kubiak, C.; Mehdi, I.; Chattopadhyay, G. Evaluation of 3D Printing Technology for Corrugated Horn Antenna Manufacturing. In Proceedings of the 2016 IEEE International Symposium on Electromagnetic Compatibility (EMC), Ottawa, ON, Canada, 25–29 July 2016.
45. Kyovtorov, V.; Georgiev, I.; Margenov, S.; Stoychev, D.; Oliveri, F.; Tarchi, D. New Antenna Design Approach—3D Polymer Printing and Metallization. Experimental Test at 14–18 GHz. *AEU Int. J. Electro. Comm.* **2017**, *73*, 119–128. [CrossRef]
46. Ghorbani, F.; Beyraghi, S.; Shabanpour, J.; Oraizi, H.; Soleimani, H.; Soleimani, M. Deep neural network-based automatic metasurface design with a wide frequency range. *Sci. Rep.* **2021**, *11*, 7102. [CrossRef]
47. Bauerle, R.J.; Schrimpf, R.; Gyorko, E.; Henderson, J. The use of a dielectric lens to improve the efficiency of a dual-polarized quad-ridge horn from 5 to 15 GHz. *IEEE Trans. Antennas Propag.* **2009**, *57*, 1822–1825. [CrossRef]
48. Türk, A.S.; Keskin, A.K.; Şentürk, M.D. Dielectric loaded TEM horn-fed ridged horn antenna design for ultrawideband ground-penetrating impulse radar. *Turkish J. Elec. Eng. Comp. Sci.* **2015**, *23*, 1479–1488. [CrossRef]
49. Belen, M.A.; Mahouti, P. Realization of dielectric sheets for gain improvement of ultra-wideband horn antennas using 3D printer technology. *Appl. Comput. Electromag. Soc. J.* **2019**, *34*, 760–764.
50. Türk, A.S.; Keskin, A.K. Partially dielectricloaded ridged horn antenna design for ultrawideband gain and radiation performance enhancement. *IEEE Antennas Wirel. Propag. Lett.* **2012**, *11*, 921–924. [CrossRef]

51. Cicchetti, R.; Cicchetti, V.; Faraone, A.; Foged, L.; Testa, O. A Wideband High-Gain Dielectric Horn-Lens Antenna for Wireless Communications and UWB Applications. *IEEE Trans. Ant. Prop.* **2023**, *71*, 1304–1318. [CrossRef]
52. Yu, W.; Peng, L.; Liu, Y.; Zhao, Q.; Jiang, X.; Li, S. An Ultrawideband and High-Aperture-Efficiency All-Dielectric Lens Antenna. *IEEE Antennas Wirel. Prop. Lett.* **2021**, *20*, 2442–2446. [CrossRef]
53. Goode, I.; Saavedra, C.E. 3D Printed Linearly Polarized X-Band Conical Horn Antenna and Lens. *IEEE Open J. Ant. Prop.* **2022**, *3*, 549–556. [CrossRef]
54. Zhang, Z.-Y.; Lu, K.; Leung, K.W. Gain Enhancement of Horn Antenna Using a Metal Lens. *IEEE Trans. Ant. Prop.* **2023**, *71*, 1337–1349. [CrossRef]
55. Marzall, L.; Danielson, P.; Lasser, G.; Popovic, Z. Broadband Small-Aperture High-Gain Ridge Horn Antenna Array Element. *IEEE Antennas Wirel. Prop. Lett.* **2021**, *20*, 708–712. [CrossRef]